Exploring carbonate rock wettability across scales: Role of (bio)minerals

Alicia Moya, Fabienne Giraud, Valerie Molinier, Yves Perrette, Laurent Charlet, Alexander van Driessche, Alejandro Fernandez-Martinez

Exploring carbonate rock wettability across scales: role of (bio)minerals

Alicia Moya[a,b*], Fabienne Giraud[a], Valerie Molinier[c], Yves Perrette[d], Laurent Charlet[a], Alexander Van Driessche[a,e], Alejandro Fernandez-Martinez[a]

[a]Univ. Grenoble Alpes, Univ. Savoie Mont Blanc, CNRS, IRD, IFSTTAR, ISTerre, 38000 Grenoble, France.
[b]Department of Inorganic Chemistry, Universidad Autónoma de Madrid, 28049, Madrid, Spain.
[c]TotalEnergies, Pôle Etudes et Recherche de Lacq, RN117, 64170 Lacq, France.
[d]CNRS, Univ. Savoie Mont Blanc, EDYTEM, 73370 Le Bourget du Lac, France.
[e]Instituto Andaluz de Ciencias de la Tierra (IACT), CSIC – Universidad de Granada, 18100 Armilla, Spain.

Abstract

Hypothesis: The wettability of carbonate rocks is expected to be affected by the organic components of biominerals which are complex, nanostructured organo-mineral assemblages, whose surfaces have a potential influence on wetting properties. Elucidating the nanoscale mechanisms driving the wettability of solid surfaces will enable a better understanding and/or control of various geological, environmental and industrial processes.

Experiments: Using Atomic Force Microscopy and Spectroscopy (AFM/AFS) we probed the wettability properties of carbonate rocks with different amounts of organic material. The adhesion properties of two types of limestones were determined in liquid environments at different length scales (nm to mm) using functionalized tips with different chemical groups to determine the extent of surface hydrophobic and hydrophilic organo-mineral interactions.

Findings: We observed homogeneous hydrophobic areas at length scales below <5 µm. The origin of this hydrophobicity is linked to the presence of organics, whose amount and spatial distribution depend on the rock composition. Specifically, our results reveal that the biogenic vs. non-biogenic origin of the mineral grains is the main rock property controlling the wettability of the solid surface. Overall, our methodology offers a multi-scale approach to unravel the role that organic moieties and biominerals play in controlling the wettability of rock-water interfaces.

Keywords: wettability, carbonates, biominerals, adhesion force, AFM/AFS

1. Introduction

Wettability is one of the key properties controlling fundamental physicochemical interfacial processes in fields such as the environmental sciences, geology, biology, material science and civil engineering. This includes the fluid transport of organic pollutants in the subsurface,[1] radwaste geological storage,[2] nucleation and growth of biominerals,[3] uptakes of nutrients by plant roots,[4] development of novel filtration systems with high physical stability[5], geological CO_2 sequestration,[6,7] enhanced oil recovery,[8] proton exchange membrane in fuel cells,[9] water desalination systems,[10,11] or conversion of CO_2 in the cement and concrete industry.[12]

The term wettability describes the preference of a solid surface to be in contact with one type of liquid rather than another one, which is essentially determined by intermolecular attractive interactions (adhesion forces).[13] Although wettability is very often reduced to hydrophilic (water-wet) and hydrophobic (oil-wet) behaviors,[14] this simplification is masking the complexity present at real surfaces, especially when investigating heterogeneous systems such as natural rocks. Most commonly, rock wettability is determined macroscopically using contact angle measurements.[15–20] However, the question arises if this type of measurement is representative of the wettability of complex systems where the surface heterogeneities are smaller than the droplet size (~0.05 mL) that is deposited on the rock surface. Probing molecular interactions at the rock-water interface could shed light on this matter, providing not only fundamental insights on the influence that such heterogeneities have on the rock wettability at the nanoscale but also the physical and chemical mechanisms behind the complex concept of surface wettability.

Surface imaging and molecular interactions can be determined in liquid media with Atomic Force Microscopy (AFM) and Spectroscopy (AFS). In AFS, an array of force-distance measurements between the AFM tip and the sample surface are recorded, from which adhesion forces can be extracted (**Fig. 1**). In addition, the functionalization of the AFM tips with organic moieties allows discerning mechanistic insights into the interactions between specific organic functionalities and the scanned surfaces.[21–23] This approach has led to significant progress in the exploration of rock wettability at the atomic scale during the last few years.[24–28] For example, various AFS studies on minerals have demonstrated the different wetting behavior induced by adsorbed or

dissolved ions (e.g. Mg^{2+} or SO_4^{2-}) or the presence of adsorbed organic matter.[29–35] Nevertheless, little attention has been paid to understanding the physical and chemical properties of the natural rock components, which will ultimately control the wettability in natural environments.

The ubiquitous presence in the nature of carbonate rocks and their abundant industrial uses have resulted in extensive research on the comprehension of their wettability.[36–38] However, carbonate rocks are highly heterogeneous in terms of surface roughness, porosity and chemical composition,[39,40] and despite many years of study, there is still not a general description of their wetting behavior. Importantly, carbonate rocks are usually formed through sedimentation processes, via the accumulation and lithification of fragments of micro-organism remains, which results in a large variety of structures, compositions – potentially including organic matter – and textures made of fossilized biominerals.[41] Biominerals are natural nanocomposite materials, composed of a hierarchical organization of organic molecules and a mineral matrix. This organization leads to the inherent heterogeneity of carbonate rocks down to the nanoscale.[42–44] Elucidating the role of the organic-inorganic nanostructures of the biominerals is paramount to understand the wettability of the rock surfaces, a task up to now never studied.

Here, we present a detailed investigation of molecular interactions at the carbonate rock-water interface using AFM/AFS (**Fig. 1A**). We have simultaneously measured topography and adhesion force maps (**Fig. 1B**) of the carbonate rock surfaces where each pixel corresponds to a single force-distance curve (**Fig. 1C**). From these curves, we determine the intermolecular – attractive or repulsive – forces between the sample and the tip either during the approach (position 1 in **Fig. 1C**) or retract step of the tip (position 2 in **Fig. 1C**). To measure hydrophobic/hydrophilic forces at the molecular level, that is, to evaluate the solid wettability properties, we used AFM tips coated with a monolayer of alkyl chains with non-polar (-CH_3, **Fig. 1D**) and polar (-COOH, **Fig. 1E**) end functional groups, that is, hydrophobic and hydrophilic nature, respectively. We performed this study from the microscale —where bioclasts can be identified— to the nanoscale and evaluated the relevant spatial scale where areas with heterogeneous surface wettability can be observed.

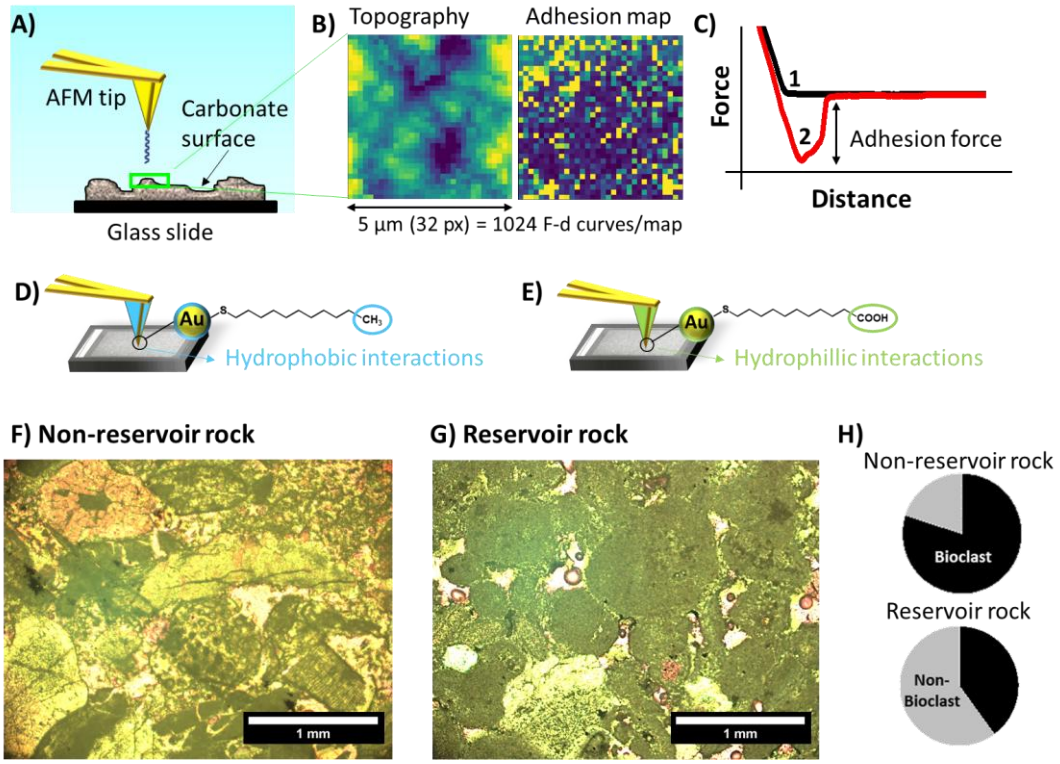

Fig. 1. A) Schematic representation of the functionalization strategy used in this work by using AFM tips to measure intermolecular forces (adhesion forces) at the rock-water interface. We used non-polished thin sections of the carbonate rocks and performed AFS experiments where B) topographical and adhesion force maps are obtained. Each pixel of those maps corresponds to force-distance curves as the one represented in C). We used AFM tip coated with alkyl chains with D) methyl (-CH_3) and E) carboxyl acid (-COOH) end groups to study hydrophobic and hydrophilic interactions, respectively. F) Optical image of the non-reservoir and G) reservoir rock took using plane-polarized light (PPL) and H) pie chart containing the percentage of bioclasts (in black) for each rock which shows a higher content of bioclasts in the non-reservoir rock which are quite well-preserved.

The samples under study are two limestone rocks, one from southern France – a non-reservoir rock (**Fig. 1F**) – and one from the Guinea gulf – an oil reservoir rock (**Fig. 1G**). The non-reservoir rock is a limestone sample with a rudstone-packstone texture, with different types of porosity, and mainly composed of bioclast-type grains (echinoderms, bryozoans, red algae, mollusks, small benthic foraminifera). The reservoir rock is a limestone sample with a grainstone-packstone texture, with different types of porosity, and is mainly composed of peloid-type grains and a few bioclast-type grains (echinoderms, mollusks). The use of these two contrasting rocks with significant differences in the bioclastic abundance (**Fig. 1H**) as well as in the adsorbed organic matter (potentially higher in the oil reservoir rock), allows determining the effect on wetting properties of foreign organic matter over the organic remains inherent from the bioclasts. Importantly, our observations at the nanoscale are carefully performed in

selected regions previously identified from optical microscopy and classified as bioclast (fragments from identified biomineral remains) vs. non-bioclast (fragments non-recognized as having a direct biomineral origin, likely peloids or intraclasts from diagenetic recrystallization) grains. This approach allows for unraveling the role of organic matter and the role of biominerals in the wettability of carbonate rocks.

2. Materials and methods

2.1. Materials

Blocs of limestone samples were provided by TotalEnergies collected from South East France (a non-reservoir limestone) and central Africa (a reservoir limestone). The non-reservoir limestone was formed during the Upper Tertiary period, Miocene epoch, Burdigalian stage. It comprises mostly calcite (>99%) with traces of quartz. This limestone is a bioclastic carbonate rock with a dual porosity system with macro and micropores (inter- and intragranular) and dual pore throats distribution with a maximum of ~6.8 and ~0.2 microns. Its specific area is ~0.46 m^2/g, the total porosity is around 32% and permeability is ~100-300 mD. The reservoir limestone is a medium to coarse oncoidal-bioclastic grainstone of mostly calcite (>95%) with dual porosity (inter- and intragranular porosity) and dual pore throats distribution with a maximum at ~10 and ~0.1 microns. Its total porosity is around 20% and permeability is ~100-200 mD. The core of both limestones was washed with toluene and isopropanol before their use to avoid any possible organic contaminant. Thin sections (40 μm thick) were used for all the experiments shown in this work. These sections were non-covered and non-polished to modify as less as possible the topographical and surface features of the different components of the carbonate rocks.

2.2. Characterization of materials

A polarizing light microscope (Olympus) was employed at 5-10X magnification for petrographic observations and paleontological identification of the constituents of the carbonate rock. Phase analysis was performed using X-Ray Diffraction (XRD), Bruker D 8 Advance v1 on the carbonate thin sections using Cu Kα radiation. Raman spectra were obtained with a LabRAM Soleil Horiba Raman microspectrometer with 532 nm wavelength laser-excitation and 1 μm spot size. Peaks were fitted using mixed Lorentzian functions using Quasar software.[45] A laser power of 15 mW was used,

which we confirmed to be sufficiently low to avoid damage in the sample by the laser. Fluorescence spectra were obtained with an experimental device for stationery and time-resolved fluorescence. Both fluorescence spectra were acquired by a nanosecond pulsed YAG laser beam excitation (266 and 355 nm, 1µJ). The sample was set on two axes translation stage to achieve fluorescence maps. With a confocal optical set-up, the 15 µm focused beam excited the sample orthogonally and the fluorescence scattering is analyzed by a monochromator (Jobin, Yvon Micro HR) and detected with a back-illuminated CCD (Syncerity S10420). Spectra were simulated by a linear combination of lognormal curves with a MATLAB script (least square fit). With the same set-up for excitation, the detection of fluorescence decay was measured by the way of a filter wheel and a Photomultiplier device (Hamamatsu H9305-01). The electric signal was recorded with an oscilloscope after pre-amplification (200 mHz of bandwidth). This detection setup allows the detection of decay longer than 5 ns. After correction, decays were simulated by way of an exponential fit and a power-like law (Jakub Wlodarczyk and Borys Kierdaszuk, 2003) (MATLAB script).

2.3. *Contact angle measurements*

Static contact angles were measured on the untreated thin sections of the reservoir rock and of the non-reservoir rock. The measurements were performed with a Tracker Tensiometer from Teclis at room temperature. 2 µL-drops of brine (composition: NaCl=32.3 g/L; $MgCl_2.6H_2O$=12.6 g/L; $CaCl_2.2H_2O$=1.7 g/L) were deposited on the samples using an automatic procedure. 12 and 7 drops were deposited in line for the non-reservoir rock and the reservoir rock respectively, to have statistical results. For all drops, the contact angle was measured after 120s.

2.4. Atomic Force Microscopy and Spectroscopy

The topographical features of the limestone sample were evaluated using Atomic Force Microscopy (AFM) operating in contact and dynamic mode.[46] All measurements were performed using a MFP-3D microscope from Asylum Research (Santa Barbara, USA) with a maximum planar range of the piezo scanner of 120 µm in the planar direction (x,y) and 15 µm in the vertical direction (z). The microscope is isolated inside a chamber and further, it contains a vibration isolation control unit from Herzan. Complementary, the AFM contains an inverted optical microscope mounted on

the AFM head that enables to record optical images of the cantilever and the sample. All the AFM images were acquired by using triangular silicon nitride (PNP-TR from NanoWorld) with a nominal length of 200 µm, a width of 28 µm, and a thickness of 500 nm. The employed AFM probes had a nominal spring constant of 0.08 $N \cdot m^{-1}$ and were routinely calibrated using the thermal method. All the obtained images were processed using the AR and WSxM software.[47]

Owing to the ability of thiols to form self-assembled monolayers (SAMs) on certain gold substrates, we functionalized gold-coated AFM tips (PNP-TR-Au from NanoWorld) with 35 nm of gold coating. The functionalization protocol starts with a UV/O_3 plasma treatment to clean gold coated-AFM tips for 20 minutes and after that, the tips are immersed into a 2mM ethanolic solution of the desired thiol for at least 24 hours. In this work, we have used undecanethiol and 11-mercaptoundecanoic acid to obtain hydrophobic and hydrophilic AFM tips, respectively. We used these functionalized tips to measure adhesion force maps of 32 x 32 px (a pixel corresponds to the region where a force-distance curve is measured and from where adhesion force is determined), containing thus 1024 force-distance curves for each adhesion force map. We further covered different spatial scales from 60 µm to 1 µm which corresponds to spectral resolutions from 2 µm/px to 30 nm/px.

All the force spectroscopy measurements were performed in low salinity conditions (1 mM NaCl solution) using a loading force of 2 nN to avoid damage to the hydrocarbon monolayer. We also checked if we unintentionally modified the rock surface by depositing the organic monolayer of the functionalized tip during the AFS measurements across the scales which were performed keeping the same center and just reducing the image size. Thus, we routinely measured again the largest area (60 µm x 60 µm) and confirmed that neither the adhesion force nor the surface roughness of the carbonate surface was not altered by the force spectroscopy measurements (**Fig. S1**).

3. Results and discussion

3.1. Does the scale of observation play a role in determining the wettability of carbonate rocks?

When studying the wettability properties of heterogeneous surfaces, such as carbonate rocks, the scale of observation can play an important role. At the macroscale,

we measured the contact angle of our carbonate rocks (**Fig. S2**). For the non-reservoir and reservoir rocks, we obtained average values of 63.8 ± 3.4° and 73.4 ± 3.9° (mean ± SD) respectively, which indicates a more hydrophobic behavior of the reservoir rock, although information about any potential heterogeneities is unavailable at this point. Observations of both limestone rocks using SEM and polarizing optical microscopy enabled the identification of the biologic constituents, as exemplified by the red algae fragment of the non-reservoir rock sample (**Fig. 2A-C**). Such identification is fundamental for further measurements of the wettability properties of individual components of the carbonate rock from the micro- to the nano-scale.

To study the molecular interactions at the rock-water interface, we performed AFS experiments on the limestone surfaces over a spatial range from 60 µm down to 1 µm, covering thus spatial resolutions from 2 µm/px to 30 nm/px. Making use of an optical microscope integrated into the AFM unit, we intentionally placed the tip in the region of interest for the wettability measurements (**Fig. 2C**) and imaged the carbonate surface at different scales (**Fig. 2D,E**). We used CH_3-functionalized tips to directly probe hydrophobic interactions by simultaneously measuring the surface topography and adhesion force maps of the surface of carbonate bioclasts (i.e. red algae in **Fig. 2F,G** and for other examples **Fig. S3**). From the topography maps, we determined the surface roughness of the rock, which decreased across the scales from 500 to 80 nm, while from adhesion force maps we observed minor differences across the studied spatial scales (**Fig. S4**). Only below 5 µm image size, we observe homogeneous hydrophobic regions which are highlighted with a contoured red dotted line in **Fig. 2G**. Although the influence of surface roughness on the macroscopic wettability properties has been reported previously,[48,49] we did not observe such a roughness effect on the adhesion data in the studied spatial resolution (**Fig. S5**). This suggests that nano-wettability is rather influenced by differences in the chemical composition of the rock surface. Overall, these results confirm that the scale of observation is an important parameter when studying rock surface wettability.

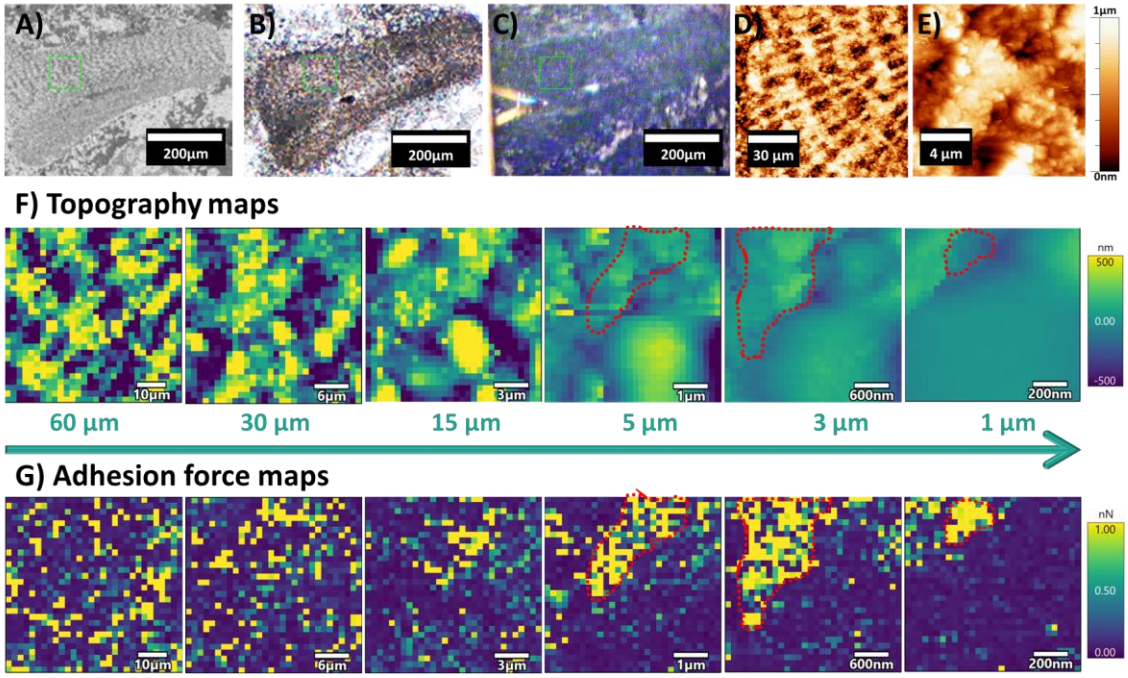

Fig. 2. Images of a bioclast of the non-reservoir rock that contains a red algae fragment obtained by: A) SEM, B) PPL optical microscope and C) inverse optical microscope coupled with AFM microscope and where the AFM tip is also presented. D,E) AFM images of the red algae area highlighted with a green square in images A-C at 120 and 20 µm image size. E) Topography and F) adhesion force maps obtained with a hydrophobic tip in a range of image sizes from 60 to 1 µm, covering resolutions of 2 µm/px to 30 nm/px. Only below an image size of 5 µm, we observe homogeneous hydrophobic regions (highlighted with a contoured dotted line in red).

3.2. Does adsorbed organic matter play a role in the wettability of carbonate rocks?

Once the relevant scale of observation is identified, the nano-wettability of the limestone rocks was explored using image sizes of 5 µm (where we observed homogeneous hydrophobic regions) and acquiring force maps with a resolution of 150 nm/px. The adhesion properties of the non-reservoir (**Fig. 3A**) and a reservoir (**Fig. 3B**) rock samples were studied using CH_3- and COOH-functionalized tips as non-polar and polar probes to mimic hydrophobic and hydrophilic organic-carbonate interactions, respectively. Representative adhesion force maps obtained with the CH_3-tip (**Fig. 3C,D**) show higher adhesive-type interactions than those obtained with COOH-tip (**Fig. 3E,F**). This is due to the higher ligand density of methyl groups enabling a better surface coverage of the AFM tip that leads to larger adhesion values, expressed as mean ± SE. The hydrophobic interactions are especially pronounced in the reservoir rock as evidenced by the larger adhesion force data (1.73 ± 0.29 nN) found in comparison to that of the non-reservoir rock (0.68 ± 0.09 nN). In addition to the preferential interaction of the reservoir rock surface with non-polar molecules, this rock type presents a highly homogeneous surface in terms of wetting behavior. In contrast, the non-reservoir rock

presents distinct homogeneous sizes of hydrophobic and hydrophilic properties. Furthermore, our measurements with COOH-tips led to slightly higher adhesion force in the non-reservoir rock (0.74 ± 0.1 nN) than in the reservoir rock (0.68 ± 0.09 nN). Looking at representative force-distance curves of both carbonate rocks using CH_3- and COOH-tips (**Fig. S6**), we observed that the approaching curves usually present electrostatic repulsion with the exception when the CH_3-tip is approaching to reservoir rock surface, which usually presents Van der Waals interactions. The adhesion peaks in the retracting curves correspond to the hydrophobic or hydrophilic interactions depending on the use of CH_3- or COOH-tips. The reservoir rock surface presents the largest adhesion peak when interacting with the CH_3-tip (7.4 nN), whereas a very small adhesion peak is observed when using COOH-tip (0.1 nN), confirming its predominant hydrophobic character. However, similar (low) adhesion peaks are observed in the interactions of the hydrophobic and hydrophilic tips with the non-reservoir rock (1.2 and 0.7 nN, respectively), ascribed to a lower content of organic matter.

Statistical analysis of our AFS results (about 250.000 force-distance curves for both rocks and both functionalized tips) was done to obtain representative wettability data of the rock surface from nanoscale interactions. The statistical results are presented as adhesion histograms in **Fig. 3G,H** and confirm the stronger hydrophobic behavior of the reservoir rock in comparison with that of the non-reservoir rock. In agreement with the macroscopic contact angle measurements (**Fig. S2**), these nanoscale measurements reveal the critical role that foreign organic matter (i.e. oil) plays in controlling the surface wettability.

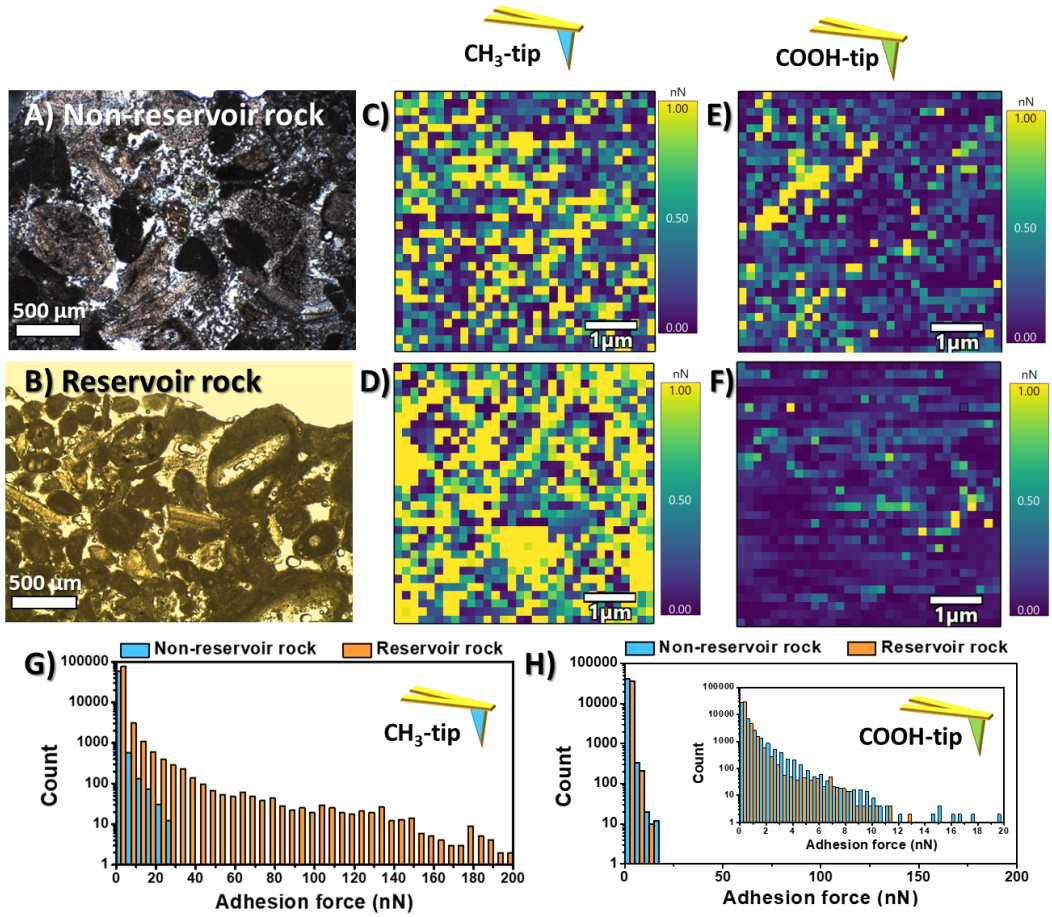

Fig. 3. Thin section optical images of A) non-reservoir and B) reservoir carbonate rocks where AFS measurements were performed. Representative adhesion force maps were obtained in both rocks using the hydrophobic (C,D) and hydrophilic (E,F) tips. Adhesion force histograms corresponding to 75000 force-curve data G) CH_3-tip and H) COOH-tip.

3.3. Is the wettability linked to the biogenicity of a rock fragment?

Hydrophobic interactions of both carbonate rocks were further explored and related to their biological origin, classifying them into different types of bioclasts. Before AFS measurements (**Fig. 4A**), the carbonate thin sections were observed with a polarizing optical microscope to identify the components of the rocks (**Fig. 4B**). We classified the rock components as bioclasts or skeletal grains with biological origin and non-bioclast including non-skeletal grains and types of cement. Then, we explored if the bioclasts influence the rock wettability of the non-reservoir and reservoir rocks using AFM and an integrated optical microscope (**Fig. 4C**). Although trivial, the identification of rock constituents from the micro- to the nano-scale has been fundamental to understand the wettability properties of the rocks. The topography and adhesion force maps of **Fig. 4D-G** show larger hydrophobic regions in the bioclast regions (**Fig. 4D-E**) than in the non-bioclasts ones (**Fig. 4F-G**). In fact, we calculated from multiple force maps that the

adhesive region in bioclasts corresponds to 47% of the imaged area, while for non-bioclasts it only represents 13% (**Fig. 4H**). Furthermore, adhesion histograms, corresponding to the analysis of 150.000 force-distance curves (**Fig. 4I**), confirm that bioclast regions interact more strongly with the hydrophobic tip than the non-bioclast ones. However, we did not observe any relevant inter-biomineral differences, i.e. echinoderm, mollusk, foraminifera, bryozoan and red algae all displayed comparable values of adhesion (**Fig. S7**).

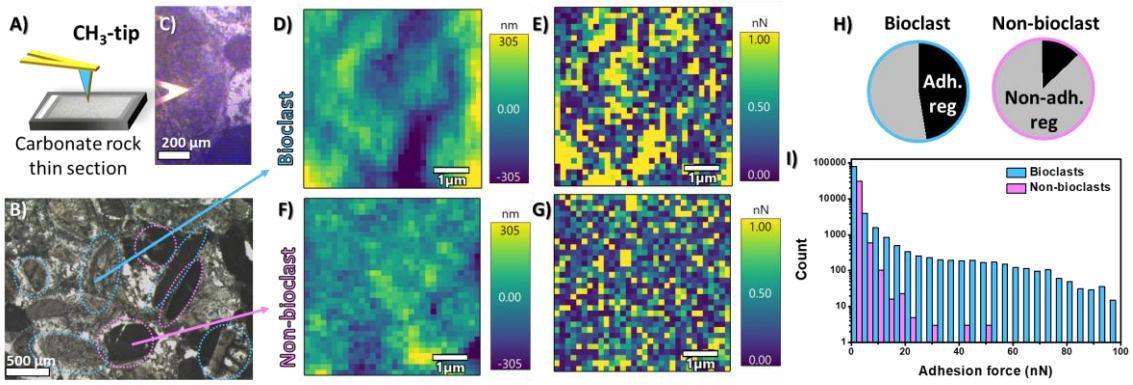

Fig. 4. A) Schematic representation of the AFS measurements using CH_3-tips and carbonate thin sections. B) Optical micrograph of the non-reservoir carbonate rock thin section. D) Topography and E) adhesion force maps of bioclasts in comparison with F) topography and G) adhesion force maps of non-bioclasts. H) Pie-chart representing the percentage of adhesion region measured over the total map area for bioclasts and non-bioclasts. I) Adhesion force histograms of the AFS measurements.

The significant difference in the wettability (**Fig. S8**) between bioclasts (0.80 and 2.89 nN for non-reservoir and reservoir rock) and non-bioclasts (0.56 and 1.35 nN for non-reservoir and reservoir rock) can be ascribed to the presence of organic remains within the former (indeed, biominerals are composite organo-mineral materials). The organic remainders favor interactions with non-polar organic molecules. Fossilized biominerals can therefore induce hydrophobicity, also facilitating the adsorption of organic matter (i.e. in oil reservoirs) through non-polar interactions.

3.4. Evaluating the role of organic matter on the wettability properties of carbonate rocks.

Based on our nanoscale observations, we have established that a more hydrophobic behavior is present in the reservoir rock. Furthermore, we have observed a significant difference between the wetting properties of bioclast and non-bioclast grains. These results highlight the key role that organic matter, either adsorbed hydrocarbons from

crude oil or gas or the breakdown products of biomolecules included in biominerals, plays on the wettability (hydrophobicity) of rock surfaces. To identify the presence of organic matter in the carbonate rock surface, we performed Raman microspectroscopy on thin sections of both limestone rocks. In addition to the calcite peaks in the low wavenumber region (calcite is the dominant calcium carbonate polymorph –**Fig. S9**), we also detected the fingerprints of organic matter in the higher wavenumber region (**Fig. 5A**). In particular, we observed the characteristic D and G bands of graphitic structures, which are attributed to in-plane defects and sp^2 C-C stretching vibrations within the aromatic rings of the graphitic layer, respectively.[50] The presence of wide D and G bands with similar intensities indicates the presence of disordered organic matter in all the samples. However, their distribution on the surface differs: the bioclasts, non-bioclasts and cement components of the reservoir rock present a homogeneous distribution on the rock surface (**Fig. S10**). But, for the non-reservoir rock, the signal from organic matter was only presented in the bioclastic grains. These results support the idea that the presence of organic matter from a natural origin is responsible for the hydrophobic behavior. Also, these maps with a resolution of 1 µm/px agree well with the spatial heterogeneity observed in the wetting properties at small spatial scales.

The position and broadening of D and G bands were determined by simultaneous peak fitting to Lorentzian profiles after baseline correction to remove the fluorescence contribution of the organic matter using Quasar software[45] (**Fig. 5B**). Based on the Raman observations in the bioclasts of the non-reservoir rock (**Fig. 5C**), the position of the G band at 1580 cm^{-1} corresponds to that of crystalline graphitic structure and the D band at 1347 cm^{-1} of high intensity indicates the presence of heteroatoms such as hydrogen, nitrogen or oxygen in the aromatic rings of the organic matter.[51] For the reservoir rock, we observed a significant blue-shift in the D and the G bands, being larger for the bioclasts (1375 and 1595 cm^{-1}) than for the non-bioclasts, including grains and cements (1370 and 1591 cm^{-1}). The shift in the G peak has been attributed to the presence of hydrocarbons adsorbed on the rock surface from the crude oil.[52] The G peaks of the bioclasts are also narrower than those of the non-bioclast grains and cements (**Fig. S11**), which reveals a higher degree of graphitization of the organic molecules in the bioclast grains. This effect is also reflected in the shift of the D peak of

the reservoir rock, which has been previously attributed to a higher degree of maturation of the organic matter in rocks.[53]

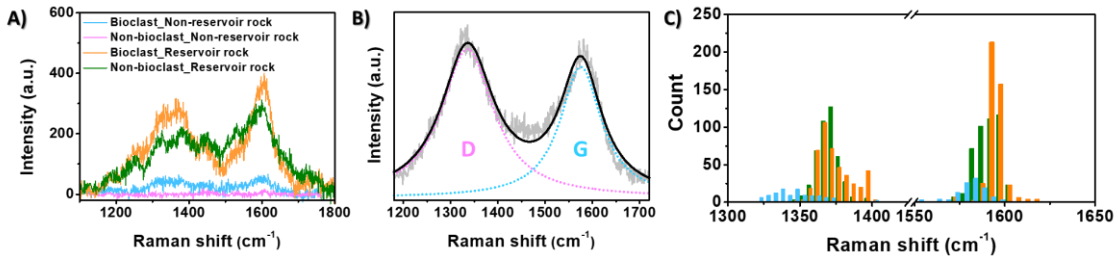

Fig. 5. A) Raman spectra of C-signal region for the bioclasts and non-bioclasts of (including grains and cements) non-reservoir and reservoir rocks. B) Example of a double Lorentzian fit ascribed to the D (pink) and G (blue) bands of graphitic structures. C) Distributions of D and G band position obtained from Raman mapping of 10 x 10 µm x µm spatial areas with a resolution of 0.5 µm for the bioclasts of the non-reservoir rock (blue) and the bioclasts (orange) and non-bioclasts (green) of the reservoir rock.

Additionally, we explored the fluorescence of organic matter contained in our carbonate rocks in the wavelength range of 300-800 nm using an excitation wavelength of 266 nm. We explored a large area of 18 mm^2 on thin sections of both carbonate rocks to observe the emission of the different components. Fluorescence intensity maps at 340 nm (**Fig. 6A**) and 420 nm (**Fig. 6B**) of non-reservoir and reservoir rocks reveal that the former contribution is characteristic of the bioclast grains. Here, the spatial resolution of the fluorescence maps does not allow for the observation of heterogeneities in the nanoscale but still gives relevant insights into the composition of the organic matter of the carbonate rocks. **Fig. 6C** shows representative spectra of bioclast and non-bioclast grains in both rocks and their fits. The fit results clearly show the presence of the peak around 340 nm (purple line) in the bioclasts – especially that of the reservoir rock – whereas it is negligible for the non-bioclasts. The fluorescence around 420 nm (blue line) is the main component of all the rock constituents. This peak is considerably wider in the bioclasts, attributed to the presence of multiple fluorophores although less intense than in the non-bioclasts. Finally, we observed a third contribution (magenta line) with an emission center around 500 nm in the bioclasts and shifted to 450 nm in the case of the non-bioclasts grains.

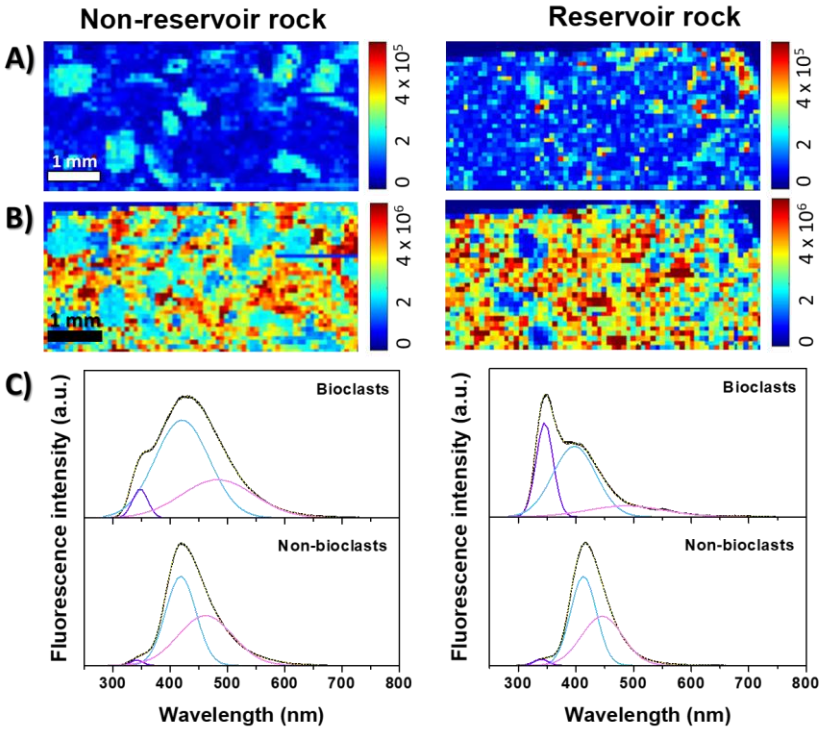

Fig. 6. Stationary fluorescence intensity maps for wavelengths of A) 340 and B) 450 nm for non-reservoir (left) and reservoir rocks (right) with a resolution of 100 µm. C) Representative fluorescence spectra of bioclasts and non-bioclasts for non-reservoir (left) and reservoir rocks (right) together to their fit using 3 gaussian peaks around 340 (purple), 420 (blue) and 500 nm (magenta).

We have further measured decay spectra in the bioclasts and non-bioclast grains of both rocks for the three contributions observed in the stationary fluorescence. The decay times were simulated with Powerlike function estimations[54] for each of the center wavelengths using and passband filter with 10 nm wavelength width. For the 340 and the 420 nm bands, decay times are low and close to the detection limit of our setup, typically between 5 and 6 ns. These results suggest that the fluorescence at 340 and 420 nm could correspond to small organic molecules rather than polyaromatic molecules which are known to exhibit a long-time decay fluorescence.[55,56] The 500 nm centered band shows a longer fluorescence decay time on the bioclast, longer than 8 ns whereas, for non-bioclast, fluorescence decay time remains between 5 and 6 ns. Furthermore, we observed a high sensitivity of the contribution around 340 and 420 nm to photodegradation (**Fig. S12**) whereas the contribution around 500 nm remains constant. This result together with the longer time decay on bioclast indicates that some hydrophobic compounds such as protein-like or humic-like (also referred to as unidentified natural organic compounds – UNOC) are present in the carbonate rocks and partially trapped by the bioclasts.[57,58] Overall, we found that bioclasts show a

different fluorescence spectrum than that of the non-bioclasts with a contribution around 340 nm that furthermore, becomes the main component in the reservoir rock. Since these results are highly in concordance with the wettability of the bioclasts, we ascribe the emission at 340 nm to organic matter of organic behavior with a plausible biological origin.

4. Conclusion

There is a common use to describe the wettability of a surface sample by using contact angle measurements. However, the macro-scale approach of such measurements only provides an average bulk value of the solid surface, missing thus valuable information from the nanoscale. Our approach to probing molecular interactions within carbonate rocks allows elucidating the complexity of rock surface wettability, especially in heterogeneous natural systems, by exploring surface heterogeneities from the micro- to the nano-scale. We demonstrate that the scale of observation is an important parameter when describing the wettability properties of natural rocks, being necessary to explore areas below 25 μm^2 to study heterogeneities of the carbonate rock in terms of wetting behavior. At this length scale, preferential interaction (stronger adhesion force) with hydrophobic molecules showed a homogeneous wetting behavior of the reservoir rock. However, at the same length scale, the non-reservoir rock presented heterogeneous hydrophobic regions only at the surface of biominerals. Furthermore, our methodology with the identification of individual components of the carbonate rock from the micro- to the nano-scale has been fundamental to explore the wettability of specific bioclast and non-bioclast grains resulting that the former presenting higher hydrophobic behavior. Such hydrophobicity can be induced in the bioclast grains by facilitating the adsorption of organic matter through non-polar interactions. The combination of adhesion force maps with micro-Raman and fluorescence spectroscopy maps have confirmed the hypothesis that organic remains within the biominerals are the main responsible for the hydrophobic character of bioclast grain surfaces. The fluorescence emission of the carbonate rocks corresponds mainly to organic matter which experiments photobleaching at long time exposition. The main signals correspond to protein-like or humic-like compounds and their short decay times reveal that small molecules with certain aromaticity are present in the rock. A high degree of maturation, observed in the position of the C signal in the Raman spectra, elucidates that small molecules with natural origin (i.e. amino acids) can be present within the rock which

leads to homogeneous hydrophobic regions. All results together highlight the critical role that the biogenic origin of the minerals plays in the wetting behavior of the studied limestones at the nanoscale, which had never been studied up to now. Furthermore, this could be used as a potential parameter to control the wettability properties of carbonate-water interfaces.

CRediT authorship contribution statement

Alicia Moya: Investigation, Data curation, Visualization, Formal analysis, Methodology, Validation, Writing – original draft, Writing – review & editing. **Fabienne Giraud:** Investigation, Validation, Writing – review & editing. **Valerie Molinier:** Investigation, Resources, Writing – review & editing. **Yves Perrette:** Investigation, Data curation, Formal analysis, Methodology, Writing – review & editing. **Laurent Charlet:** Conceptualization, Resources, Supervision, Funding acquisition, Writing – review & editing. **Alexander Van Driessche:** Conceptualization, Resources, Supervision, Funding acquisition, Writing – review & editing. **Alejandro Fernandez-Martinez:** Conceptualization, Resources, Supervision, Funding acquisition, Writing – review & editing.

Data availability

The data that support the plots within this paper and other findings of this study are available from the corresponding author upon reasonable request.

Declaration of Competing Interest

The authors declare no competing interests.

Acknowledgments

We thank Ms. Laura Pauliet for performing the contact angle measurements in TotalEnergies laboratories. We acknowledge funding from Labex OSUG@2020 Equipment.

Appendix A. Supporting material

Supplementary data to this article can be found online at

References

[1] J.W.N. Smith, D.N. Lerner, Geomorphologic control on pollutant retardation at the groundwater–surface water interface, Hydrol. Process. 22 (2008) 4679–4694. https://doi.org/10.1002/hyp.7078.

[2] B. Ma, L. Charlet, A. Fernandez-Martinez, M. Kang, B. Madé, A review of the retention mechanisms of redox-sensitive radionuclides in multi-barrier systems, Appl. Geochem. 100 (2019) 414–431. https://doi.org/10.1016/j.apgeochem.2018.12.001.

[3] S. Elhadj, J.J.D. Yoreo, J.R. Hoyer, P.M. Dove, Role of molecular charge and hydrophilicity in regulating the kinetics of crystal growth, Proc. Natl. Acad. Sci. 103 (2006) 19237–19242. https://doi.org/10.1073/pnas.0605748103.

[4] E.M. Dettenmaier, W.J. Doucette, B. Bugbee, Chemical Hydrophobicity and Uptake by Plant Roots, Environ. Sci. Technol. 43 (2009) 324–329. https://doi.org/10.1021/es801751x.

[5] U. Hübner, C. Wurzbacher, D.E. Helbling, J.E. Drewes, Engineering of managed aquifer recharge systems to optimize biotransformation of trace organic chemicals, Curr. Opin. Environ. Sci. Health. 27 (2022) 100343. https://doi.org/10.1016/j.coesh.2022.100343.

[6] C.J. Bronick, R. Lal, Soil structure and management: a review, Geoderma. 124 (2005) 3–22. https://doi.org/10.1016/j.geoderma.2004.03.005.

[7] A. Raza, R. Gholami, M. Sarmadivaleh, Feasibility of limestone reservoirs as a carbon dioxide storage site: An experimental study, AAPG Bull. 104 (2020) 83–96. https://doi.org/10.1306/04241918124.

[8] A. Gandomkar, M.R. Rahimpour, Investigation of Low-Salinity Waterflooding in Secondary and Tertiary Enhanced Oil Recovery in Limestone Reservoirs, Energy Fuels. 29 (2015) 7781–7792. https://doi.org/10.1021/acs.energyfuels.5b01236.

[9] R. Anderson, L. Zhang, Y. Ding, M. Blanco, X. Bi, D.P. Wilkinson, A critical review of two-phase flow in gas flow channels of proton exchange membrane fuel cells, J. Power Sources. 195 (2010) 4531–4553. https://doi.org/10.1016/j.jpowsour.2009.12.123.

[10] O. Lehmann, L. Birnhack, O. Lahav, Design aspects of calcite-dissolution reactors applied for post treatment of desalinated water, Desalination. 314 (2013) 1–9. https://doi.org/10.1016/j.desal.2012.12.017.

[11] D. Hasson, L. Fine, A. Sagiv, R. Semiat, H. Shemer, Modeling Remineralization of Desalinated Water by Micronized Calcite Dissolution, Environ. Sci. Technol. 51 (2017) 12481–12488. https://doi.org/10.1021/acs.est.7b03069.

[12] M. Lim, G.-C. Han, J.-W. Ahn, K.-S. You, Environmental Remediation and Conversion of Carbon Dioxide (CO2) into Useful Green Products by Accelerated Carbonation Technology, Int. J. Environ. Res. Public. Health. 7 (2010). https://doi.org/10.3390/ijerph7010203.

[13] E.C. Donaldson, W. Alam, CHAPTER 1 - Wettability, in: E.C. Donaldson, W. Alam (Eds.), Wettability, Gulf Publishing Company, 2008: pp. 1–55. https://doi.org/10.1016/B978-1-933762-29-6.50007-7.

[14] I. Gupta, J. Jernigen, M. Curtis, C. Rai, C. Sondergeld, Water-Wet or Oil-Wet: is it Really That Simple in Shales?, Petrophysics - SPWLA J. Form. Eval. Reserv. Descr. 59 (2018) 308–317. https://doi.org/10.30632/PJV59N3-2018a2.

[15] H.J. Deglint, C.R. Clarkson, C. DeBuhr, A. Ghanizadeh, Live Imaging of Micro-Wettability Experiments Performed for Low-Permeability Oil Reservoirs, Sci. Rep. 7 (2017) 4347. https://doi.org/10.1038/s41598-017-04239-x.

[16] A. Ivanova, N. Mitiurev, A. Cheremisin, A. Orekhov, R. Kamyshinsky, A. Vasiliev, Characterization of Organic Layer in Oil Carbonate Reservoir Rocks and its Effect on Microscale Wetting Properties, Sci. Rep. 9 (2019) 10667. https://doi.org/10.1038/s41598-019-47139-y.
[17] M.A.Q. Siddiqui, S. Ali, H. Fei, H. Roshan, Current understanding of shale wettability: A review on contact angle measurements, Earth-Sci. Rev. 181 (2018) 1–11. https://doi.org/10.1016/j.earscirev.2018.04.002.
[18] M. Seyyedi, M. Sohrabi, A. Farzaneh, Investigation of Rock Wettability Alteration by Carbonated Water through Contact Angle Measurements, Energy Fuels. 29 (2015) 5544–5553. https://doi.org/10.1021/acs.energyfuels.5b01069.
[19] W. Abdallah, A. Gmira, Wettability Assessment and Surface Compositional Analysis of Aged Calcite Treated with Dynamic Water, Energy Fuels. 28 (2014) 1652–1663. https://doi.org/10.1021/ef401908w.
[20] K. Huang, P. Rowe, C. Chi, V. Sreepal, T. Bohn, K.-G. Zhou, Y. Su, E. Prestat, P.B. Pillai, C.T. Cherian, A. Michaelides, R.R. Nair, Cation-controlled wetting properties of vermiculite membranes and its promise for fouling resistant oil–water separation, Nat. Commun. 11 (2020) 1097. https://doi.org/10.1038/s41467-020-14854-4.
[21] R. Barattin, N. Voyer, Chemical modifications of AFM tips for the study of molecular recognition events, Chem. Commun. (2008) 1513–1532. https://doi.org/10.1039/B614328H.
[22] Y. Xia, Y. Xing, M. Li, M. Liu, J. Tan, Y. Cao, X. Gui, Studying interactions between undecane and graphite surfaces by chemical force microscopy and molecular dynamics simulations, Fuel. 269 (2020) 117367. https://doi.org/10.1016/j.fuel.2020.117367.
[23] W. Zhang, H. Yang, F. Liu, T. Chen, G. Hu, D. Guo, Q. Hou, X. Wu, Y. Su, J. Wang, Molecular interactions between DOPA and surfaces with different functional groups: a chemical force microscopy study, RSC Adv. 7 (2017) 32518–32527. https://doi.org/10.1039/C7RA04228K.
[24] Hassenkam T., Skovbjerg L. L., Stipp S. L. S., Probing the intrinsically oil-wet surfaces of pores in North Sea chalk at subpore resolution, Proc. Natl. Acad. Sci. 106 (2009) 6071–6076. https://doi.org/10.1073/pnas.0901051106.
[25] D. Afekare, J.C. Garno, D. Rao, Insights into Nanoscale Wettability Effects of Low Salinity and Nanofluid Enhanced Oil Recovery Techniques, Energies. 13 (2020). https://doi.org/10.3390/en13174443.
[26] J. Wu, F. Liu, H. Yang, S. Xu, Q. Xie, M. Zhang, T. Chen, G. Hu, J. Wang, Effect of specific functional groups on oil adhesion from mica substrate: Implications for low salinity effect, J. Ind. Eng. Chem. 56 (2017) 342–349. https://doi.org/10.1016/j.jiec.2017.07.030.
[27] S. Yesufu-Rufai, M. Rücker, S. Berg, S.F. Lowe, F. Marcelis, A. Georgiadis, P. Luckham, Assessing the wetting state of minerals in complex sandstone rock in-situ by Atomic Force Microscopy (AFM), Fuel. 273 (2020) 117807. https://doi.org/10.1016/j.fuel.2020.117807.
[28] S. Yesufu-Rufai, F. Marcelis, A. Georgiadis, S. Berg, M. Rücker, J. van Wunnik, P. Luckham, Atomic Force Microscopy (AFM) study of redox conditions in sandstones: Impact on wettability modification and mineral morphology, Colloids Surf. Physicochem. Eng. Asp. 597 (2020) 124765. https://doi.org/10.1016/j.colsurfa.2020.124765.
[29] T. Hassenkam, C.S. Pedersen, K. Dalby, T. Austad, S.L.S. Stipp, Pore scale observation of low salinity effects on outcrop and oil reservoir sandstone, Colloids

572 Surf. Physicochem. Eng. Asp. 390 (2011) 179–188.
573 https://doi.org/10.1016/j.colsurfa.2011.09.025.
574 [30] J. Matthiesen, N. Bovet, E. Hilner, M.P. Andersson, D.A. Schmidt, K.J. Webb,
575 K.N. Dalby, T. Hassenkam, J. Crouch, I.R. Collins, S.L.. S. Stipp, How Naturally
576 Adsorbed Material on Minerals Affects Low Salinity Enhanced Oil Recovery,
577 Energy Fuels. 28 (2014) 4849–4858. https://doi.org/10.1021/ef500218x.
578 [31] E. Hilner, M.P. Andersson, T. Hassenkam, J. Matthiesen, P.A. Salino, S.L.S.
579 Stipp, The effect of ionic strength on oil adhesion in sandstone – the search for the
580 low salinity mechanism, Sci. Rep. 5 (2015) 9933.
581 https://doi.org/10.1038/srep09933.
582 [32] B. Lorenz, M. Ceccato, M.P. Andersson, S. Dobberschütz, J.D. Rodriguez-Blanco,
583 K.N. Dalby, T. Hassenkam, S.L.S. Stipp, Salinity-Dependent Adhesion Response
584 Properties of Aluminosilicate (K-Feldspar) Surfaces, Energy Fuels. 31 (2017)
585 4670–4680. https://doi.org/10.1021/acs.energyfuels.6b02969.
586 [33] N.R. Pedersen, T. Hassenkam, M. Ceccato, K.N. Dalby, K. Mogensen, S.L.S.
587 Stipp, Low Salinity Effect at Pore Scale: Probing Wettability Changes in Middle
588 East Limestone, Energy Fuels. 30 (2016) 3768–3775.
589 https://doi.org/10.1021/acs.energyfuels.5b02562.
590 [34] J. Generosi, M. Ceccato, M.P. Andersson, T. Hassenkam, S. Dobberschütz, N.
591 Bovet, S.L.S. Stipp, Calcite Wettability in the Presence of Dissolved Mg2+ and
592 SO42–, Energy Fuels. 31 (2017) 1005–1014.
593 https://doi.org/10.1021/acs.energyfuels.6b02029.
594 [35] J. Matthiesen, T. Hassenkam, N. Bovet, K.N. Dalby, S.L.S. Stipp, Adsorbed
595 Organic Material and Its Control on Wettability, Energy Fuels. 31 (2017) 55–64.
596 https://doi.org/10.1021/acs.energyfuels.6b00627.
597 [36] S. Mann, Molecular recognition in biomineralization, Nature. 332 (1988) 119–124.
598 https://doi.org/10.1038/332119a0.
599 [37] M.P. Andersson, K. Dideriksen, H. Sakuma, S.L.S. Stipp, Modelling how
600 incorporation of divalent cations affects calcite wettability–implications for
601 biomineralisation and oil recovery, Sci. Rep. 6 (2016) 28854.
602 https://doi.org/10.1038/srep28854.
603 [38] M. Shakeel, P. Pourafshary, M. Rehan Hashmet, Hybrid Engineered Water–
604 Polymer Flooding in Carbonates: A Review of Mechanisms and Case Studies,
605 Appl. Sci. 10 (2020). https://doi.org/10.3390/app10176087.
606 [39] M. Dernaika, M. Al Mansoori, M. Singh, T. Al Dayyani, Z. Kalam, R. Bhakta, S.
607 Koronfol, Y.N. Uddin, Digital and Conventional Techniques to Study Permeability
608 Heterogeneity in Complex Carbonate Rocks, Petrophysics - SPWLA J. Form.
609 Eval. Reserv. Descr. 59 (2018) 373–396. https://doi.org/10.30632/PJV59N3-
610 2018a6.
611 [40] A. Hosa, R. Wood, Order of diagenetic events controls evolution of porosity and
612 permeability in carbonates, Sedimentology. 67 (2020) 3042–3054.
613 https://doi.org/10.1111/sed.12733.
614 [41] W.J. Kennedy, Trace Fossils in Carbonate Rocks, in: R.W. Frey (Ed.), Study Trace
615 Foss. Synth. Princ. Probl. Proced. Ichnology, Springer Berlin Heidelberg, Berlin,
616 Heidelberg, 1975: pp. 377–398. https://doi.org/10.1007/978-3-642-65923-2_17.
617 [42] A.M.J. Fichtinger-Schepman, J.P. Kamerling, J.F.G. Vliegenthart, E.W. De Jong,
618 L. Bosch, P. Westbroek, Composition of a methylated, acidic polysaccharide
619 associated with coccoliths of Emiliania huxleyi (Lohmann) Kamptner, Carbohydr.
620 Res. 69 (1979) 181–189. https://doi.org/10.1016/S0008-6215(00)85763-8.

[43] Zamarreño Dania V., Inkpen Robert, May Eric, Carbonate Crystals Precipitated by Freshwater Bacteria and Their Use as a Limestone Consolidant, Appl. Environ. Microbiol. 75 (2009) 5981–5990. https://doi.org/10.1128/AEM.02079-08.
[44] Y.-Y. Kim, K. Ganesan, P. Yang, A.N. Kulak, S. Borukhin, S. Pechook, L. Ribeiro, R. Kröger, S.J. Eichhorn, S.P. Armes, B. Pokroy, F.C. Meldrum, An artificial biomineral formed by incorporation of copolymer micelles in calcite crystals, Nat. Mater. 10 (2011) 890–896. https://doi.org/10.1038/nmat3103.
[45] M. Toplak, G. Birarda, S. Read, C. Sandt, S.M. Rosendahl, L. Vaccari, J. Demšar, F. Borondics, Infrared Orange: Connecting Hyperspectral Data with Machine Learning, Synchrotron Radiat. News. 30 (2017) 40–45. https://doi.org/10.1080/08940886.2017.1338424.
[46] P.J. de Pablo, J. Colchero, M. Luna, J. Gómez-Herrero, A.M. Baró, Tip-sample interaction in tapping-mode scanning force microscopy, Phys. Rev. B. 61 (2000) 14179–14183. https://doi.org/10.1103/PhysRevB.61.14179.
[47] I. Horcas, R. Fernández, J.M. Gómez-Rodríguez, J. Colchero, J. Gómez-Herrero, A.M. Baro, WSXM: A software for scanning probe microscopy and a tool for nanotechnology, Rev. Sci. Instrum. 78 (2007) 013705. https://doi.org/10.1063/1.2432410.
[48] A.M. Alhammadi, A. AlRatrout, K. Singh, B. Bijeljic, M.J. Blunt, In situ characterization of mixed-wettability in a reservoir rock at subsurface conditions, Sci. Rep. 7 (2017) 10753. https://doi.org/10.1038/s41598-017-10992-w.
[49] X. Wang, Q. Zhang, Insight into the Influence of Surface Roughness on the Wettability of Apatite and Dolomite, Minerals. 10 (2020). https://doi.org/10.3390/min10020114.
[50] M.A. Pimenta, G. Dresselhaus, M.S. Dresselhaus, L.G. Cançado, A. Jorio, R. Saito, Studying disorder in graphite-based systems by Raman spectroscopy, Phys. Chem. Chem. Phys. 9 (2007) 1276–1290. https://doi.org/10.1039/B613962K.
[51] Y. Wang, D.C. Alsmeyer, R.L. McCreery, Raman spectroscopy of carbon materials: structural basis of observed spectra, Chem. Mater. 2 (1990) 557–563. https://doi.org/10.1021/cm00011a018.
[52] J.S. Riedeman, N.R. Kadasala, A. Wei, H.I. Kenttämaa, Characterization of Asphaltene Deposits by Using Mass Spectrometry and Raman Spectroscopy, Energy Fuels. 30 (2016) 805–809. https://doi.org/10.1021/acs.energyfuels.5b02002.
[53] Q.H.S. Chan, A. Stephant, I.A. Franchi, X. Zhao, R. Brunetto, Y. Kebukawa, T. Noguchi, D. Johnson, M.C. Price, K.H. Harriss, M.E. Zolensky, M.M. Grady, Organic matter and water from asteroid Itokawa, Sci. Rep. 11 (2021) 5125. https://doi.org/10.1038/s41598-021-84517-x.
[54] J. Włodarczyk, B. Kierdaszuk, Kinetics of triplet excitation transport in disordered organic solids, Chem. Phys. 297 (2004) 139–142. https://doi.org/10.1016/j.chemphys.2003.10.021.
[55] J. René Albani, Fluorescence Lifetimes of Tryptophan: Structural Origin and Relation with So → 1Lb and So → 1La Transitions, J. Fluoresc. 19 (2009) 1061. https://doi.org/10.1007/s10895-009-0506-7.
[56] M. Rasouli, S.H. Tavassoli, S.J. Mousavi, S.M.R. Darbani, Measuring of naphthalene fluorescence emission in the water with nanosecond time delay laser induced fluorescence spectroscopy method, Optik. 127 (2016) 6218–6223. https://doi.org/10.1016/j.ijleo.2016.04.081.

669 [57] J.F. Power, R. LeSage, D.K. Sharma, C.H. Langford, Fluorescence lifetimes of the
670 well characterized humic substance, armdale fulvic acid, Environ. Technol. Lett. 7
671 (1986) 425–430. https://doi.org/10.1080/09593338609384429.
672 [58] V. Bresler, V. Yanko, Chemical ecology; a new approach to the study of living
673 benthic epiphytic Foraminifera, J. Foraminifer. Res. 25 (1995) 267–279.
674 https://doi.org/10.2113/gsjfr.25.3.267.
675

676